Analysis of passively automatic air inlets for livestock buildings

M.R.L. BANTLE[1], E.M. BARBER[2] and G.R. BAYNE[3]

[1]*Bantle Engineering Research, P.O. Box 7805, Saskatoon, SK, Canada S7K 4R5; Department of Agricultural Engineering, University of Saskatchewan, Saskatoon, SK, Canada S7N 0W0; and Agricultural Engineering Branch, Saskatchewan Agriculture & Food, Regina, SK, Canada S4S 0B1.* *Received 28 August 1990; accepted 7 February 1991.*

Bantle, M.R.L., Barber, E.M. and Bayne, G.R. 1991. **Analysis of passively automatic air inlets for livestock buildings.** Can. Agric. Eng. **33**:363-371. The aerodynamic moment acting on a hinged baffle of a passively automatic air inlet was measured for three different flow configurations at pressure drops of 5, 20, 35 and 50 Pa. In two of the configurations, air entered the inlet from a plenum above the inlet, thereby simulating air entry from an attic. In the third configuration, air entered the inlet from a plenum beside the inlet, thereby simulating a sidewall inlet. When the inlet pressure drop was maintained constant, the moment acting on the inlet baffle due to airflow through the inlet (aerodynamic moment) decreased as the airflow rate increased for all three inlet configurations. This result indicates that a restraint system which exerts a constant counter moment may not be workable if a constant pressure is required. However, the condition of a constant pressure with a constant counter moment may be approached with the two attic inlet configurations provided the maximum inlet opening is restricted. The open wall configuration inlet is not suitable for use as a passively automatic inlet because the aerodynamic moment decreased very sharply for increasing airflow rates even when the inlet was only 20% open. A numerical model was developed which accurately predicted the aerodynamic moment on the baffles under conditions of low airflow rates. However, the model was not accurate for higher flow rates. It is believed that separation within the flow channel, which could not be accounted for in the model, was the major reason for the poor performance of the model at higher flow rates.

On a mesuré le moment aérodynamique agissant sur la chicane articulée d'une entrée d'air à système automatique passif, et ce, pour trois différentes configurations d'écoulement à des variations de pression de 5, 20, 35 et 50 Pa. Dans deux des cas, l'air entrait à partir d'un plenum situé au-dessus de l'entrée, simulant ainsi une ventilation par les combles. Dans le troisième cas, l'air pénétrait à partir d'un plenum situé à côté, simulant une ventilation par les murs latéraux. Lorsque la chute de pression était maintenue constante, le moment agissant sur la chicane, dû à l'écoulement d'air à travers l'entrée (moment aérodynamique), diminuait à mesure que le débit augmentait pour les trois configurations. Ce résultat indique qu'un système de retenue exerçant un moment contraire constant peut ne pas être praticable si une pression constante est nécessaire. Toutefois, il est possible d'approcher de l'état de pression constante et de moment contraire constant avec les deux configurations de ventilation par les combles, à condition que l'ouverture d'entrée maximale soit restreinte. La configuration de mur ouvert ne convient pas en tant qu'entrée à système automatique passif, parce que le moment aérodynamique diminue très brusquement avec des augmentations de débits d'air, même lorsque l'entrée n'est ouverte qu'à 20 %. On a élaboré un modèle numérique qui prévoyait de manière précise le moment aérodynamique sur les chicanes, avec de faibles écoulements d'air. Cependant, le modèle manquait de précision quand les débits étaient plus élevés. On pense que la séparation à l'intérieur du canal d'écoulement - dont on ne pouvait pas tenir compte dans le modèle - est la cause principale du faible rendement de ce dernier à des débits élevés.

INTRODUCTION

In a typical livestock building, the ventilation rate must be varied by as much as a factor of twenty between winter and summer. Much effort has been expended to develop automatic control of fans to achieve automatically this modulation of airflow rate. Much less effort has gone into automation of air inlets.

Experience has indicated that poor air distribution and drafts result from improper adjustment of air inlets. Therefore, some form of automation is required. Complete automation of inlets, fully synchronized with the operation of fans, can be achieved with modern microprocessor-based controllers; however, such control systems are expensive and have not been widely adopted to date in Canada. Gravity shutters, spring-loaded baffles, and counterweighted baffles, such as those illustrated in Fig. 1, are conceptually appealing as a low cost way to automate air inlets. However, field experience has indicated that these passively automatic inlets do not always provide proper airflow modulation from summer to winter and that the pressure difference across the inlets may vary too much as the ventilation rate changes.

The objectives of this project were to measure the aerodynamic moment on the inlet baffle of three commonly used inlet configurations, to develop a theoretical model which would predict the performance of a passively automatic air inlet based on some basic test data, and to evaluate the performance of the three inlet configurations.

PREVIOUS INVESTIGATIONS OF AIR INLETS

The literature on the design of passively controlled automatic air inlets is very limited.Carson et al. (1988) studied the operation of a passive air inlet that relied on the weight of the baffle to close the baffle (similar to configuration d, Fig. 1). Theoretical predictions of the inlet performance were made assuming incompressible inviscid flow. The unique geometry of this type of inlet made it possible to model the inlet as a one-dimensional airflow problem. The model was reported to predict accurately the pressure difference and inlet jet velocities over a 10-fold range of ventilation rates. The study was limited to just the one particular inlet configuration.

Munroe et al. (1988) studied the performance of a passive air inlet (CPS Plan M-9715) similar to configuration b, Fig. 1. The adjustment of the inlet was controlled by counterweights. The authors presented only a limited theoretical analysis. Based on experimental observations, it was concluded that at

least a 10-fold range of ventilation rates could be achieved with relatively small changes in static pressure (10-15 Pa) and without changing the length of the moment arm on the counterweight. With an adjustment of the counterweight moment arm twice yearly, a 20-fold change of ventilation rate was considered possible.

Albright (1978, 1976) considered the airflow through a baffled, centre-ceiling slot inlet and a hinged-baffle slot inlet. The hinged-baffle inlet was similar to configurations b and c, Fig. 1, but without the counterweight. In both cases, dimensional analysis was used to obtain an equation which predicted the airflow rate through the inlet as a function of inlet geometry and the static pressure drop across the inlet.The results of these investigations cannot be applied directly to predict the functioning of a passively controlled air inlet because no information was given on the pressure profile across the baffle.

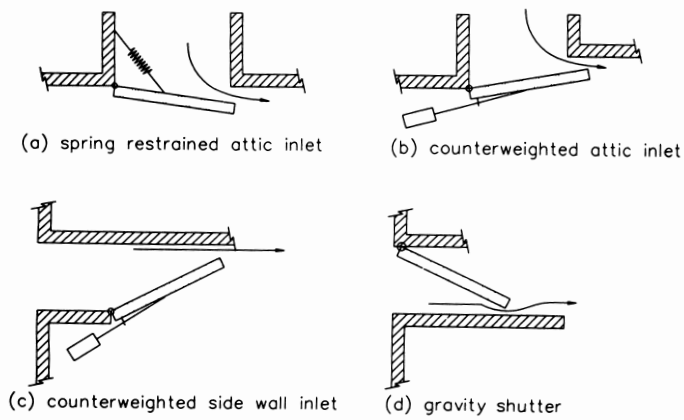

Fig. 1. Configurations of passively automatic air inlets.

DEVELOPMENT OF THE THEORETICAL MODEL

Airflow through slot air inlets in livestock buildings can be modelled as a two-dimensional flow. This assumption may not be valid for very short air inlet modules where end effects may be significant.

Because most livestock buildings are ventilated using propeller fans, the pressure drop across air inlets usually is limited to less than 50 Pa; therefore, the flow may be considered to be incompressible.

Inertial, pressure, and viscous forces are involved in the slot inlet flow problem. However, in this analysis the viscous effects were assumed to be confined to a small region next to the boundary such that the bulk of the flow could be treated as an inviscid flow. An inviscid flow implies that the fluid acceleration is due entirely to pressure differences and that the no-slip boundary condition at a solid wall must be relaxed.

If air enters the inlets from a large reservoir, as from an attic, directly through an outside wall, or from a large duct, and if the entrance to the inlet is smooth, the flow will enter with no vorticity. Once the flow is in the inlet itself, the viscous effects of the wall will cause vorticity to diffuse but if the boundary layer is small then the bulk of the fluid can be considered irrotational. The combination of an inviscid and irrotational flow is an ideal or potential flow.

For a potential flow, the shape and location of the walls of the flow passage completely establish the flow velocities and streamlines. Since the geometry controls the flow patterns, the velocity may be found without ever solving the momentum equation. The momentum equation is only used to determine the pressure field.

Flow separation invalidates the use of potential flow theory in solving a flow problem. Flow which separates and leaves the wall carries with it vorticity and viscous effects from the boundary layer. A large region of back flow or recirculating flow exists downstream of the separation and frequently leads to an unsteady turbulent wake (Panton 1984). Thus, when separation occurs, the viscous effects and the vorticity diffusion can not be assumed to be confined to a thin layer near the walls. Some specific numerical calculations of separated flow have been made but this subject still remains an unresolved area of fluid mechanics. To study the flow through a passive air inlet, the assumption of an ideal flow is thought to be acceptable if no vorticity is present in the flow upon entry to the inlet and if flow separation within the inlet is minimized.

The one-dimensional modelling approach used by Carson et al (1988) could not be applied to the two-dimensional flow channel of a generalized hinged-baffle air inlet. An alternative analytic solution procedure was sought. The flow passage through an air inlet such as shown in Fig. 1 is a polygon and thus it was expected that, with some simplification of the flow passage, it would be possible to apply the Schwarz Christoffel transformation to obtain an analytical solution. The Schwarz Christoffel transformation (Churchill et al. 1976) maps a polygon which is a closed contour in one plane to the upper half plane in another plane. This transformation permits a complicated flow in the one plane to be transformed into a simple flow in another plane for which an analytical solution exists. However, investigation of this concept indicated that even with a simplified flow passage geometry, the analytical solution became very complex. Therefore, a numerical solution was thought to be more appropriate.

The analysis of problems by numerical methods is based on approximating conditions in a continuous field by a finite number of values at discrete points. For this two-dimensional problem, the flow was divided into a two-dimensional grid of equally spaced lattice points. Figure 2 shows a typical grid. In this model development, the grid was 10 mm by 10 mm.

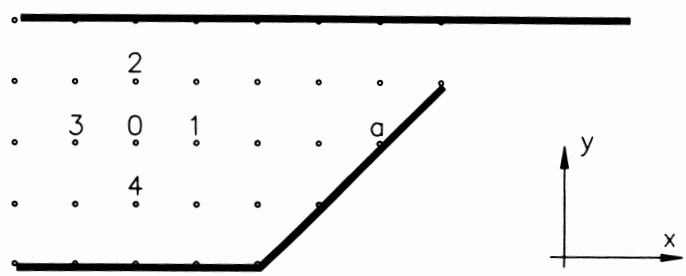

Fig. 2. Grid for numerical computation of stream function.

Stream function computation

Since the flow is an ideal flow, the stream function satisfies Laplace's Equation. The stream function at any point in the flow is the average of the stream function at four adjacent points:

$$\psi_0 = (\psi_1 + \psi_2 + \psi_3 + \psi_4)/4 \quad (1)$$

where ψ_j = stream function at position j.

Thom's Square Method (Robertson 1965) was used to solve the stream function inside the flow boundary. This method was selected because it is much faster and is more amenable to solution of large flow grids than a simple averaging of the four adjacent points.

The boundaries of the air inlets being studied have flow geometries which result in some of the lattice points in the rectangular grid lying outside the boundary of the flow channel. For example, in Fig. 3, calculation of the stream function at point "0" involves the two grid points, "1" and "2" which lie outside the boundary. The method reported by Robertson (1965) was used to calculate the stream function at a point adjacent to a boundary:

$$\psi_0 = (r\psi_1 + s\psi_2 + \psi_3 + \psi_4)/(2 + r + s) \quad (2)$$

where the scaling factors, r and s, are as shown in Fig. 3.

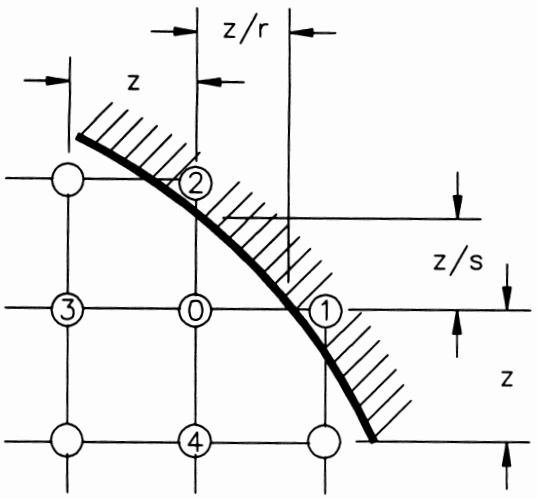

Fig. 3. Grid for computation of stream function at lattice points near the boundaries of the flow channel.

Flow velocity

The stream function was calculated at all of the lattice points in the flow field, and then the velocity was computed at the same lattice points using:

$$u = \partial\psi/\partial x \quad : \quad v = -\partial\psi/\partial y \quad (3)$$

where:

u = velocity in the x-direction (m/s), and

v = velocity in the y-direction (m/s).

The velocities of most interest were those along the baffle surface. Since the velocity can change dramatically at short distances from the boundary, it is important to compute the derivative at the boundary rather than at lattice points some short distance away from the boundary. Equation 4a (Robertson 1965) was used to calculate the velocity, v, at the boundary (refer to Fig. 4):

$$\left.\frac{\partial\psi}{\partial y}\right|_{\text{boundary}} = (1+r)\frac{\psi_0 - \psi_1}{z} - \frac{1}{1+r}\frac{\psi_0 - \psi_2}{z} \quad (4a)$$

Calculation of the velocity, u, requires interpolation to find $\psi_{a'}$ and $\psi_{a''}$ in Fig. 4, and then Eq. 4b can be applied:

$$\left.\frac{\partial\psi}{\partial x}\right|_{\text{boundary}} = (1+r)\frac{\psi_{a'} - \psi_a}{z} - \frac{1}{1+r}\frac{\psi_{a''} - \psi_a}{z} \quad (4b)$$

This procedure was repeated at equally spaced intervals along the baffle.

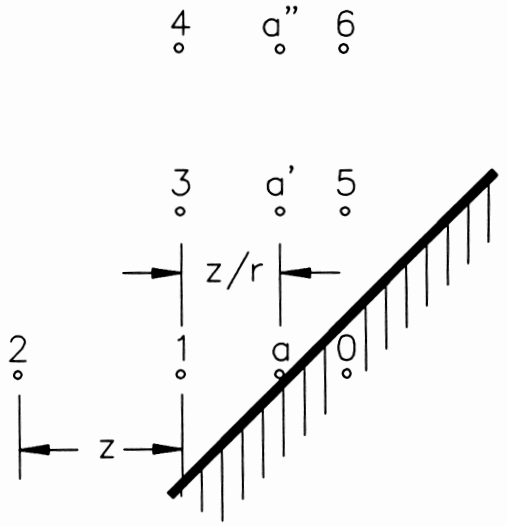

Fig. 4. Grid for computation of stream function at the boundary of the flow channel.

Aerodynamic moment

The position of the baffle in a passively automatic air inlet is determined by the balance between the aerodynamic moment exerted on the baffle by the airflow through the inlet and the counter moment developed by the restraint system. The aerodynamic moment is the result of the pressure difference between the two sides of the baffle.

For a steady, irrotational flow, the pressure and the fluid velocity are related by Bernoulli's Equation:

$$P/\rho + 0.5(u^2 + v^2) = \text{Constant} \quad (5)$$

where:

P = air pressure (Pa), and

ρ = air density (kg/m^3).

This equation was used to calculate the pressure at points along the baffle. The constant in Eq. 5 was computed by assuming that flow separation would occur at the minimum flow area in the flow passage. It then was assumed that the average pressure at this section would be equal to the pressure on the leeward side of the baffle. Since only the net pressure on the baffle was required, the pressure on the leeward side of the baffle was set equal to zero and the constant in Eq. 5 was computed from:

$$\text{Constant} = 0.5(U_{max})^2 \quad (6)$$

where

U_{max} = average air velocity at the minimum flow area (m/s).

The maximum velocity was calculated from:

$$U_{max} = q/(C_d h) \quad (7)$$

where:

q = airflow per unit length of inlet ($m^3 \cdot s^{-1} \cdot m^{-1}$),

h = the inlet opening height (m), and

C_d = discharge coefficient.

Figure 5 shows a baffle in a flow field. The moment acting on the baffle, per unit length of the baffle, with respect to the hinge at point "O" was computed from:

$$M = \sum_{i=1}^{I-1} 0.5b^2(P_i + P_{i-1})(i - 0.5) + t(P_{I-1})[0.5t + (I-1)b] \quad (8)$$

All dimensions are illustrated in Fig. 5.

In the idealization of the inlet flow, the streamlines were continued around the tip of the baffle. This simplification resulted in very high velocities at the tip. To overcome this problem, the pressure calculated at point "I" was neglected and the pressure P_{I-1} was assumed to act uniformly from the point "I-1" to the tip.

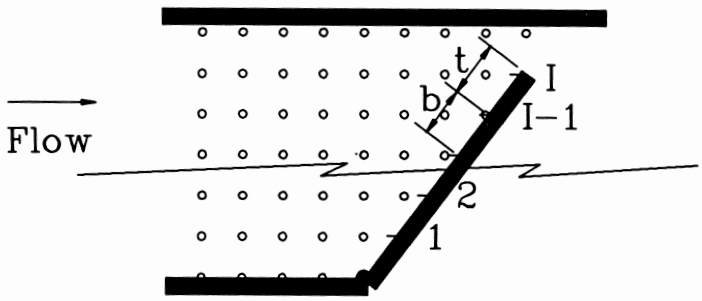

Fig. 5. Grid for computation of pressures and aerodynamic moment on the hinged inlet baffle.

EXPERIMENTAL PROCEDURE

Three inlet configurations were tested in a chamber at the University of Saskatchewan Agricultural Engineering Hardy Laboratory. Figure 6 shows the chamber and the inlet attachment positions. The original chamber had inside dimensions of 4.88 m x 2.30 m x 2.44 m, but for these tests one corner of the chamber was reconstructed to accommodate testing of an attic entry inlet configuration. In the reconstructed chamber, the distance between the roof of the test chamber and the entrance to the simulated ceiling inlet port was 0.75 m. The distance between the endwall of the test chamber and the trailing edge of that inlet port was 0.70 m. The chamber was located within a larger airspace in which the temperature was maintained relatively constant near 23°C.

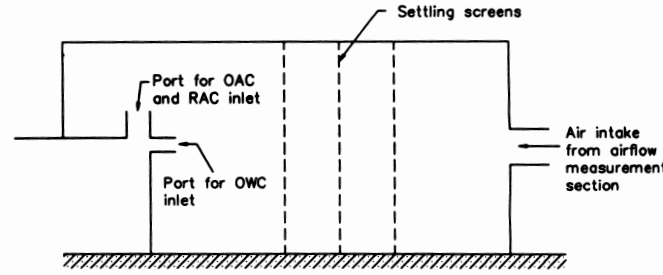

Fig. 6. Longitudinal section through the test chamber.

Air was forced through the chamber by two centrifugal fans operated by a variable speed drive. Air delivered by the fans entered the chamber through an AMCA-Standard airflow measurement section (AFMS). The AFMS consisted of six precision flow nozzles. By manually changing the combination of nozzles that were open, airflow rates of 0.04 - 1.6 m^3/s were possible. The pressure drop across the nozzles was measured using a manometer (Model MICRO 34FB2, Meriam Instruments, Zurich, Switzerland) having a resolution of ± 1.3 Pa. Air temperature was measured in the supply air duct using a precision mercury thermometer. After the air entered the chamber from the AFMS, it passed through a set of three settling screens placed there to promote uniform velocity approaching the inlet section. Previous tests indicated that leakage in the shell of the chamber was less than 0.001 m^3/s at a pressure difference of 25 Pa.

The static pressure difference across the test inlet was measured with the same manometer as that used at the AFMS. One port was open to the large laboratory outside the chamber. The other port was connected to a piezometer ring joining three pressure taps that were flush-mounted with the inside surfaces of the experimental chamber. The three pressure taps were located in the ceiling and the two side walls of the chamber.

Two ports were constructed in the chamber to which the test inlet modules were attached. The larger port was 255 x 1200 mm and simulated an air entry from an attic. The smaller port was 105 x 1200 mm and simulated an air entry through a side wall. Each port was fitted on the upstream side with a 285 mm deep entry channel to simulate an attic insulation stop or a channel through a wall.

Three of the four inlet configurations shown in Fig. 1 were tested. In the open attic configuration (OAC), the air entered the inlet from above (Fig. 7). The baffle was hinged at the ceiling and the axis of rotation of the baffle was such that the baffle was always angled away from the ceiling. At an angle of 0°, the inlet opening was 23 mm. In the restricted attic configuration (RAC), air also entered from above, but the baffle was hinged 105 mm below the ceiling. In this configuration, the baffle was always angled toward the ceiling. In the open wall configuration (OWC), air entered the inlet horizontally. As with the RAC inlet, the baffle was hinged 105 mm below the ceiling and the baffle was always angled toward the ceiling.

The inlet baffle was constructed of 2.66 mm thick aluminum plate. One edge of the baffle was attached to a 12.7 mm square shaft. The overall dimension of the baffle with the attached

shaft was 305 x 1200 mm. The trailing edge of the baffle was turned over at 90° to form a 37 mm lip and thus to simulate the thickness of polystyrene baffles that often are used in livestock buildings.

The inlet baffle was held within a mounting frame. The shaft supporting the baffle was held at both ends by two small bearings. This design was intended to minimize the counter moment due to friction at the hinge. The bearings were mounted in aluminum end plates which in turn were attached to the chamber using a mounting flange. The three different inlet configurations were achieved by changing the orientation of the end plates and the position of the hinge. The end plates were mounted to achieve a close fit between them and the ends of the baffle and thus to minimize air leakage around the ends of the baffle. Also to minimize leakage, the end plates were sealed to the chamber with duct tape. The space between the shaft and the chamber was bridged with a strip of polyethylene sheet which was taped along one edge to the chamber and along the other edge to the baffle, thus creating an airtight hinge with negligible rotational resistance.

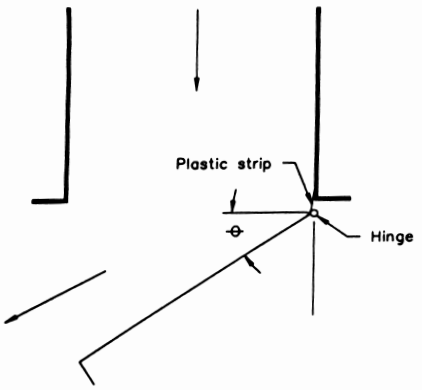

(a) Open attic configuration (OAC)

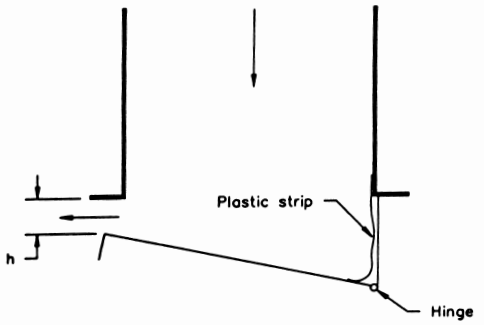

(b) Restricted attic configuration (RAC)

(c) Open wall configuration (OWC)

Fig. 7. Schematic of the three inlet configurations.

The inlet module was designed so the aerodynamic moment on the baffle could be measured accurately (Fig. 8). A 312.9 mm diameter wheel was attached to one end of the shaft which formed the hinge of the baffle. A weight was attached to the circumference of the wheel by a small diameter cable. The length of the cable was adjusted using turnbuckles. The weight was supported on an electronic scale (Model PL1200, Mettler Instruments, Cleveland, OH) and remained stationary on the scale. As air was forced through the inlet, the aerodynamic moment on the baffle tended to rotate it clockwise and thus to lift the weight off the scale. The moment due to the weight of the baffle itself was constant. Therefore, the change in the scale reading, multiplied by the moment arm (wheel radius = 0.1565 m) was a direct measure of the aerodynamic moment on the baffle.

For these tests, the baffle position and the inlet pressure drop were fixed and the airflow rate through the inlet at these conditions was measured. Data were collected at pressure drops of 5, 20, 35 and 50 Pa at each of 3 or 4 baffle positions.

A test proceeded by first adjusting the baffle and the cable and scale apparatus until the desired baffle angle was attained with nearly the full weight of the counterweight bearing on the scale. During this procedure, the airflow rate was zero. The airflow rate then was increased until the desired pressure drop was achieved, and this flow rate was measured. The baffle angle was retained at the desired value by adjustment of the turnbuckles.

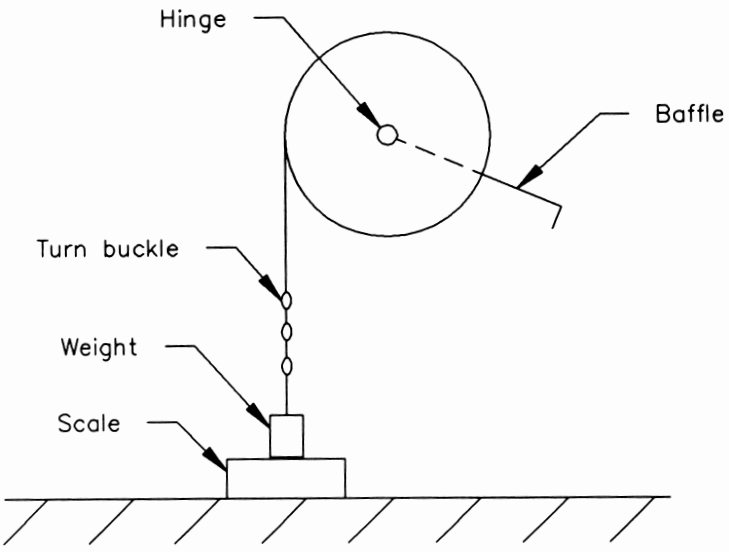

Fig. 8. Schematic of system for measuring aerodynamic moment.

RESULTS AND DISCUSSION

The experimental conditions under which each inlet was tested are summarized in Table I. The measured aerodynamic moment and the airflow rate at each of the experimental conditions are shown in Fig. 9 - 11 respectively for the OAC,

RAC and OWC inlets.

At any fixed inlet opening, both the moment and the pressure drop increased as the airflow rate increased. For a fixed pressure drop and baffle opening, the moment was larger for the RAC inlet than for the other two inlets. The RAC configuration is less efficient in providing airflow with a minimal pressure loss than are the other two, relatively more streamlined, inlet configurations.

A passively-operated air inlet baffle for cold region livestock buildings should provide a 20-fold change in air delivery rate while maintaining a nearly constant pressure drop across the inlet. Fan energy could be reduced by decreasing inlet air speeds during warm weather operation. Therefore, in some ventilation systems, it may be best if the pressure drop decreases, and hence the jet velocity decreases, as the flow rate increases. The opposite effect was shown for the three inlet configurations that were tested. That is, for a constant counter moment, the pressure drop across the inlet will increase as the inlet opens in response to higher airflow rates.

Table I. Conditions under which the inlets were tested

Inlet Configuration	Baffle Angle (deg)	Inlet Slot Height (mm)	Discharge Coefficient
OAC	0	23	0.72
	15	88	0.73
	30	148	0.68
	60	234	0.69
RAC	16	20	0.59
	8	60	0.71
	1	100	0.67
OWC	16	20	0.74
	8	60	0.94
	1	100	0.72

The results of these tests can be used in two ways. First, the data can be used to design a restraint system in which the counter moment is decreased as the airflow rate increases, while maintaining a prescribed relationship between flow rate and pressure drop. For example, the counter moment required for the OAC inlet intended to maintain a constant pressure drop of 20 Pa will decrease from 0.65 N•m/m at a flow of 0.1 $m^3 \cdot s^{-1} \cdot m^{-1}$ to 0.22 N•m/m at a flow rate of 0.9 $m^3 \cdot s^{-1} \cdot m^{-1}$. A fixed counterweight system could not be used, but a properly designed spring-restraint system could provide this modulation of the counter moment.

The second use of the data is to identify the maximum inlet opening beyond which the required counter moment for a given pressure drop decreases rapidly, or beyond which the pressure drop increases rapidly if the counter moment is held constant. The range of airflow and pressure drops for each inlet for a fixed moment are shown by the dotted lines in Fig. 9 to 11. If the OAC inlet was fitted with a constant counter moment of 0.65 N•m/m, the inlet would open to 23 mm (0°) for a flow of 0.1 $m^3 \cdot s^{-1} \cdot m^{-1}$ and a pressure drop of 20 Pa. If the flow was increased 10 fold to 1 $m^3 \cdot s^{-1} \cdot m^{-1}$, the inlet would open to approximately 45° and the pressure drop would increase to greater than 40 Pa. The data indicate that the maximum opening should be restricted to less than 15° if the pressure drop is to be kept nearly constant at 20 Pa for a fixed counter moment of 0.65 N•m/m. Similarly, for the RAC inlet, if the pressure drop is to be kept nearly constant at 20 Pa, the maximum inlet opening should be less than 60% of the fully open, horizontal

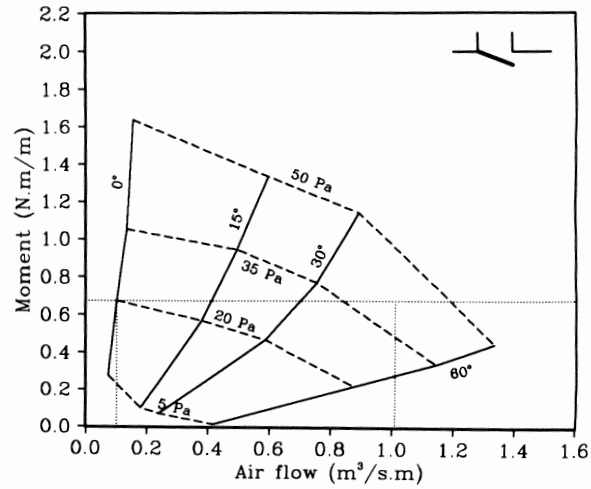

Fig. 9. Measured aerodynamic moments for OAC inlet.

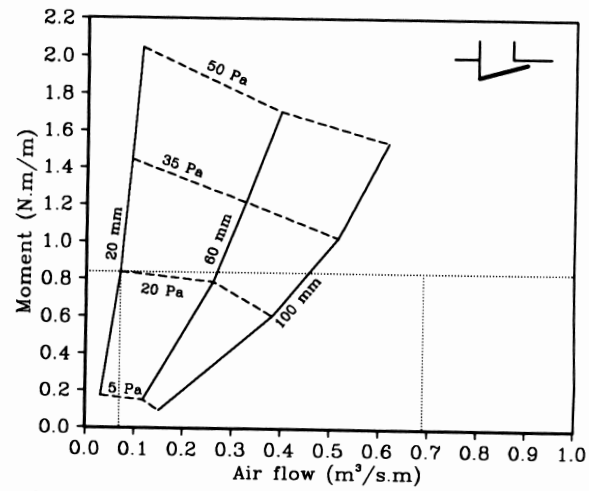

Fig. 10. Measured aerodynamic moments for RAC inlet.

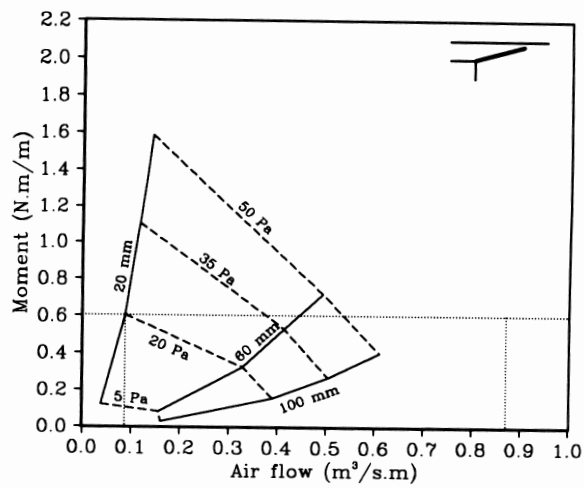

Fig. 11. Measured aerodynamic moments for OWC inlet.

baffle position. Given this restriction, the pressure drop will be nearly constant at 20 Pa for a fixed counter moment of 0.84 N•m/m. For the OWC inlet at an opening of 20 mm, or approximately 20% of the fully open, horizontal baffle position, the inlet is already beyond the opening at which a nearly constant pressure of 20 Pa is possible at a constant counter moment.

Further measurements are needed to test the performance of the three inlet configurations at inlet openings smaller than 20 mm. The relationship between inlet opening height and airflow rate is approximately linear for small inlet openings. Then, for the RAC inlet with a maximum opening of 60 mm, a minimum opening of 3 mm would be required to make possible a 20 fold modulation of ventilation rate. A similar minimum opening for the OAC inlet is also needed. Because the slope of the moment versus flow rate curve is quite flat at low flow rates, it seems possible that these two inlet configurations might afford a 20 fold modulation of ventilation rate for a constant counter moment and a constant pressure drop of 20 Pa. This hypothesis needs further testing. The OWC inlet, on the other hand, does not offer much promise as a passively automatic inlet because the aerodynamic moment at a constant pressure is strongly dependent upon the airflow rate, even at relatively small inlet openings.

COMPARISON BETWEEN PREDICTIONS AND MEASUREMENTS

The theoretical predictions were developed by specifying the flow geometry (ie., the inlet type and the baffle position) and the flow rate and then computing the aerodynamic moment acting on the inlet baffle. Two critical variables in the computation of the aerodynamic moment were the inlet pressure loss and the maximum jet velocity.

Early in the analysis of the results, it became apparent that the pressure loss at the entry into the inlet channel could not be neglected. The entrance pressure loss was calculated using:

$$\Delta P_e = 0.5\rho C_e U_e 2 \tag{9}$$

where:

ΔP_e = entrance pressure drop (Pa),

C_e = entrance pressure loss coefficient, and

U_e = entrance mean velocity (m/s).

The velocity at the entrance to the inlet, U_e, was calculated as:

$$U_e = q/b \tag{10}$$

where:

q = airflow rate per meter length of inlet ($m^3 \cdot s^{-1} \cdot m^{-1}$), and

b = width of the entrance channel (m).

The pressure loss coefficients were not measured and therefore were estimated as 0.69 for the OAC and RAC inlets and 0.50 for the OWC inlet (ASHRAE 1989).

The estimate of the maximum velocity, U_{max}, was calculated using Eq. 7. Ideally, a single discharge coefficient, C_d, would be known apriori for each inlet. However, in this analysis, C_d had to be estimated from the known values for the inlet pressure loss, P, the airflow rate, q, and the inlet slot height, h. The discharge coefficient was determined for each opening width of each inlet configuration using the linear model:

$$(\Delta P_t - \Delta P_e)_{measured} = 0.5\ \beta\ \rho(q/h)^2 \tag{11}$$

where β is the least squares estimator of C_d-2.

Estimates for C_d are given in Table I. That the RAC inlet had the lowest apparent discharge coefficient is consistent with the rather poorly streamlined shape of this flow channel compared to the other two inlet configurations. The discharge coefficient approaching 1 for the OWC inlet at an opening of 60 mm is consistent with the very streamlined shape of the inlet at that inlet opening. Because the discharge coefficient appeared to be relatively sensitive to the inlet opening for the RAC and OWC inlets, the individual estimates were used rather than an average value for each inlet type in subsequent calculations of the aerodynamic moment.

The model predictions and the measurements for inlet pressure drop and the aerodynamic moment are compared in Fig. 12 to 14. The near perfect agreement between measured and predicted pressure drop was forced by the least-squares estimation procedure for estimating an apparent discharge coefficient as outlined previously. The purpose of the model was not to predict the pressure drop, but rather to predict the aerodynamic moment given a known pressure drop.

Agreement between predictions and measurements of the aerodynamic moment for the RAC inlet was very good at all inlet openings. The fit was good for the OWC inlet at the two lowest opening widths. For the OAC inlet, the model consistently overestimated the aerodynamic moment, the size of the error increasing as the flow rate and the inlet opening height increased.

Two possible reasons were identified to explain the poor prediction of the aerodynamic moment by the model for the OAC inlet and for the OWC inlet at larger opening widths. First, whereas the model accounts for pressure losses at the entrance to the inlet, it does not account for friction losses within the inlet. Consequently, the predicted values for the maximum inlet discharge velocity may be too high. Overestimation of this maximum velocity would result in an overestimation of the pressures on the top side of the baffle and hence of the aerodynamic moment. Neglecting friction losses within the inlet, however, is not expected to have been a major contributor to the error.

The second and more significant problem is that the model assumed no separation anywhere within the flow field. For the OAC inlet, flow will separate at the exit from the entrance channel, resulting in higher velocities along the baffle surface than the model predicts. The model forces the flow to bend around the corner, spreading the flow over more area than if it separates. The higher velocities in practice will result in a lower pressure profile and a smaller aerodynamic moment. A similar effect likely occurred for the OWC inlet at maximum opening. Flow separation may have occurred at the sharp entrance to the inlet channel. For small inlet slot openings, the converging flow channel would have reduced the effects of flow separation at the entrance, but at full inlet opening the flow may not have reattached to both boundaries of the flow channel before the inlet discharge at the baffle tip.

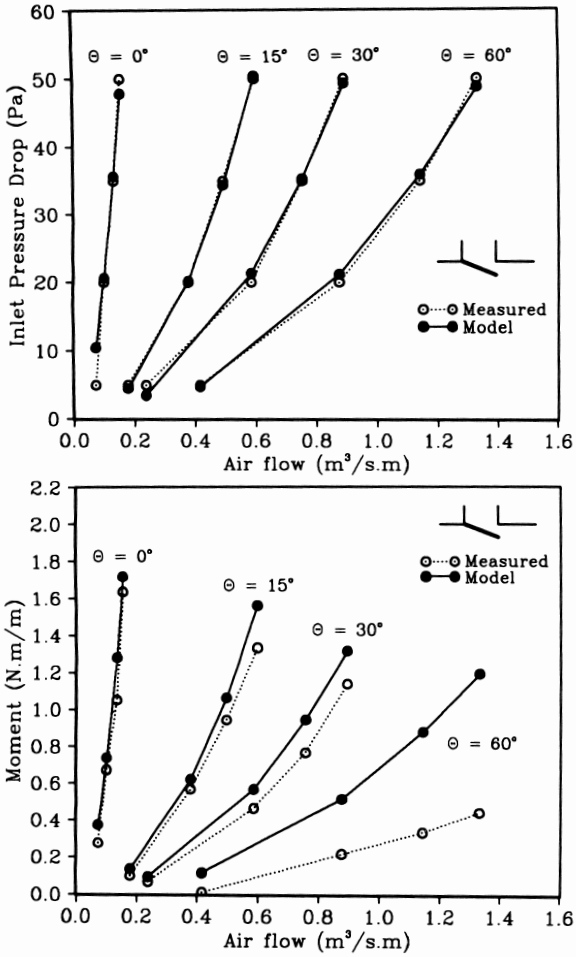

Fig. 12. Comparison between measurements and model predictions for OAC inlet.

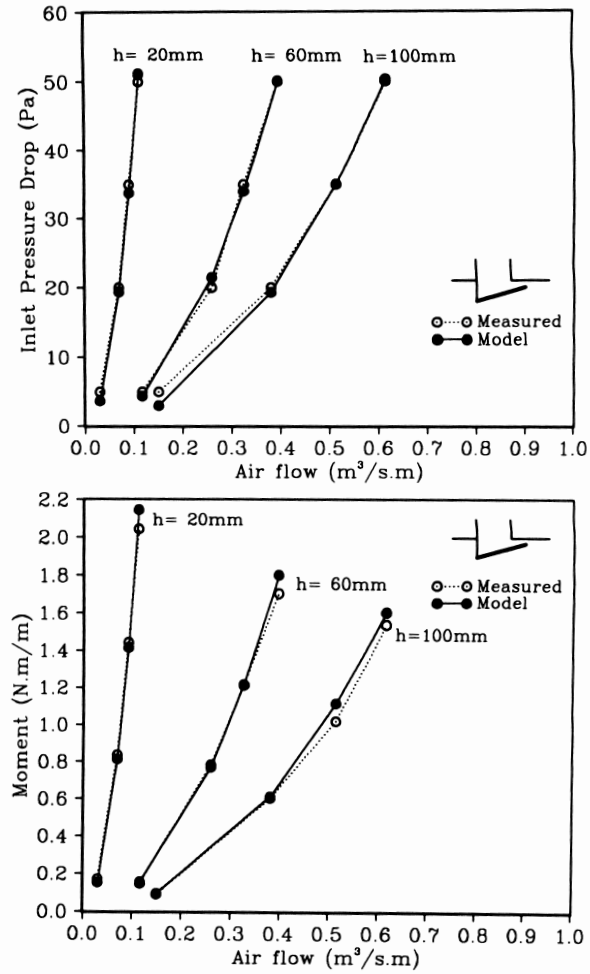

Fig. 13. Comparison between measurements and model predictions for RAC inlet.

CONCLUSIONS

Three inlet configurations were tested to determine the aerodynamic moment on the baffle as the airflow rate was modulated. A mathematical model was developed to predict the moment, given test data for the total pressure drop across the inlet. The following conclusions can be drawn as a result of this work:

(1) The test data acquired for the three inlet configurations may be used to design a restraint system for passively automatic inlets. For all three configurations, the counter moment must decrease as the flow rate increases if the inlet pressure drop is to be kept constant.

(2) Where a constant counter moment is to be used with the OAC and the RAC inlets, the extent of the pressure drop dependence on airflow rate can be minimized by limiting the maximum inlet opening. For the particular inlets tested, these limits were 15° for the OAC inlet and 60% of the fully open position for the RAC inlet. At even 20% of the fully open position, the OWC inlet exhibited a large decrease in the aerodynamic moment for small increases in airflow rate at a fixed inlet pressure drop; therefore, this inlet configuration offers little promise as a passively automatic inlet system.

(3) A numerical model was developed which accurately predicted the aerodynamic moment on the baffles for low airflow rates. However, the model was less accurate for higher flow rates. It is believed that flow separation within the flow channel, which could not be accounted for in the model, is the major reason for the poor performance of the model at higher flow rates.

ACKNOWLEDGEMENT

Funding for this project was provided by the Agriculture Development Subsidiary Agreement, Canada/Saskatchewan Economic and Regional Development Agreement, Saskatchewan Agriculture.

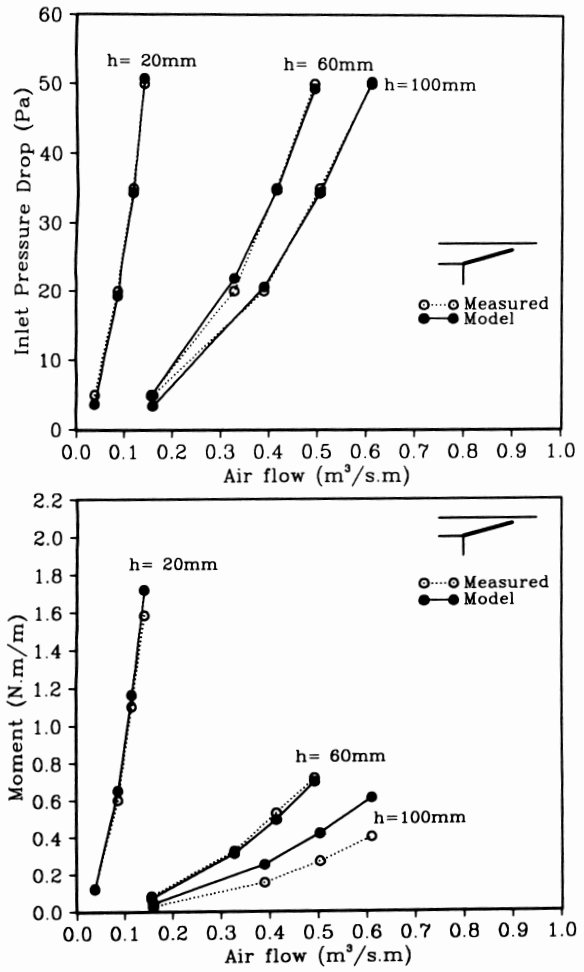

Fig. 14. Comparison between measurements and model predictions for OWC inlet.

REFERENCES

ALBRIGHT, L.D. 1976. Air flow through hinged baffle slotted inlets. Trans. ASAE 19(4):728-732, 735.

ALBRIGHT, L.D. 1978. Air flow through baffled, center-ceiling, slotted inlets. Trans ASAE 21(5):944-947, 952.

ASHRAE. 1989. Handbook of Fundamentals. Am. Soc. Heating, Refrigerating and Air Conditioning Engineers, Atlanta, GA.

CARSON, J.M., P.N. WALKER and H.B. MANBECK. 1988. Gravity controlled ventilation inlet analysis. Paper No. 88-4508. Am. Soc. Agric. Engrs., St. Joseph, MI.

CHURCHILL, R.V., J.W. BROWN and R.F. VERHEY. 1976. Complex Variables and Applications. McGraw-Hill Book Company, New York, NY.

MUNROE, J.A., J.E. TURNBULL and D.G. HODGKINSON. 1988. Performance of automatic counterbalanced air inlets with and without recirculation. In: Livestock Environment III, Proc. Third International Livestock Environment Symposium, ASAE Publ. 1-88, Am. Soc. Agric. Engrs., St. Joseph, MI.

PANTON, R.L. 1984. Incompressible Flow. John Wiley & Sons, New York, NY.

ROBERTSON, J.M.. 1965. Hydrodynamics in Theory and Application. Prentice-Hall, Inc., Englewood Cliffs, NJ.